Superlattice photonic crystal as broadband solar absorber for high temperature operation

Veronika Rinnerbauer,[1] Yichen Shen,[2] John D. Joannopoulos,[2] Marin Soljačić,[2] Friedrich Schäffler,[1] and Ivan Celanovic[2,*]

[1]*Institute of Semiconductor and Solid State Physics, Johannes Kepler University Linz, Altenbergerstr. 69, 4040 Linz, Austria*
[2]*Massachusetts Institute of Technology, 77 Massachusetts Avenue, MA, Cambridge 02139, USA*
[*]*ivanc@mit.edu*

Abstract: A high performance solar absorber using a 2D tantalum superlattice photonic crystal (PhC) is proposed and its design is optimized for high-temperature energy conversion. In contrast to the simple lattice PhC, which is limited by diffraction in the short wavelength range, the superlattice PhC achieves solar absorption over broadband spectral range due to the contribution from two superposed lattices with different cavity radii. The superlattice PhC geometry is tailored to achieve maximum thermal transfer efficiency for a low concentration system of 250 suns at 1500 K reaching 85.0% solar absorptivity. In the high concentration case of 1000 suns, the superlattice PhC absorber achieves a solar absorptivity of 96.2% and a thermal transfer efficiency of 82.9% at 1500 K, amounting to an improvement of 10% and 5%, respectively, versus the simple square lattice PhC absorber. In addition, the performance of the superlattice PhC absorber is studied in a solar thermophotovoltaic system which is optimized to minimize absorber re-emission by reducing the absorber-to-emitter area ratio and using a highly reflective silver aperture.

References and links

1. A. Lenert, D. M. Bierman, Y. Nam, W. R. Chan, I. Celanović, M. Soljačić, and E. N. Wang, "A nanophotonic solar thermophotovoltaic device," Nat. Nanotechnol. **9**(2), 126–130 (2014).
2. A. Datas and C. Algora, "Development and experimental evaluation of a complete solar thermophotovoltaic system," Prog. Photovolt. Res. Appl. **21**, 1099 (2012).
3. V. M. Andreev, A. S. Vlasov, V. P. Khvostikov, O. A. Khvostikova, P. Y. Gazaryan, S. V. Sorokina, and N. A. Sadchikov, "Solar thermophotovoltaic converters based on tungsten emitters," J. Sol. Energy Eng. **129**(3), 298 (2007).
4. A. Steinfeld, "Solar thermochemical production of hydrogen - a review," Sol. Energy **78**(5), 603–615 (2005).
5. E. Rephaeli and S. Fan, "Absorber and emitter for solar thermo-photovoltaic systems to achieve efficiency exceeding the Shockley-Queisser limit," Opt. Express **17**(17), 15145–15159 (2009).
6. V. Rinnerbauer, A. Lenert, D. M. Bierman, Y. X. Yeng, W. R. Chan, R. D. Geil, J. J. Senkevich, J. D. Joannopoulos, E. N. Wang, M. Soljačić, and I. Celanovic, "Metallic photonic crystal absorber-emitter for efficient spectral control in high-temperature solar thermophotovoltaics," Adv. Energy Mater. **4**(12), 1400334 (2014).
7. C. E. Kennedy, *Review of mid- to high-temperature solar selective absorber materials*, Tech. Rep. TP-520–31267 (National Renewable Energy, 2002).
8. E. Rephaeli and S. Fan, "Tungsten black absorber for solar light with wide angular operation range," Appl. Phys. Lett. **92**(21), 211107 (2008).
9. N. P. Sergeant, O. Pincon, M. Agrawal, and P. Peumans, "Design of wide-angle solar-selective absorbers using aperiodic metal-dielectric stacks," Opt. Express **17**(25), 22800–22812 (2009).
10. P. Bermel, M. Ghebrebrhan, W. Chan, Y. X. Yeng, M. Araghchini, R. Hamam, C. H. Marton, K. F. Jensen, M. Soljačić, J. D. Joannopoulos, S. G. Johnson, and I. Celanovic, "Design and global optimization of high-efficiency thermophotovoltaic systems," Opt. Express **18**(S3 Suppl 3), A314–A334 (2010).

11. N. P. Sergeant, M. Agrawal, and P. Peumans, "High performance solar-selective absorbers using coated sub-wavelength gratings," Opt. Express **18**(6), 5525–5540 (2010).
12. C. Argyropoulos, K. Q. Le, N. Mattiucci, G. D'Aguanno, and A. Alù, "Broadband absorbers and selective emitters based on plasmonic Brewster metasurfaces," Phys. Rev. B **87**(20), 205112 (2013).
13. J. G. Fleming, S. Y. Lin, I. El-Kady, R. Biswas, and K. M. Ho, "All-metallic three-dimensional photonic crystals with a large infrared bandgap," Nature **417**(6884), 52–55 (2002).
14. X. Yu, Y.-J. Lee, R. Furstenberg, J. O. White, and P. V. Braun, "Filling fraction dependent properties of inverse opal metallic photonic crystals," Adv. Mater. **19**(13), 1689–1692 (2007).
15. C. Wu, B. Neuner III, J. John, A. Milder, B. Zollars, S. Savoy, and G. Shvets, "Metamaterial-based integrated plasmonic absorber/emitter for solar thermo-photovoltaic systems," J. Opt. **14**(2), 024005 (2012).
16. Y. Guo, C. L. Cortes, S. Molesky, and Z. Jacob, "Broadband super-Planckian thermal emission from hyperbolic metamaterials," Appl. Phys. Lett. **101**(13), 131106 (2012).
17. S. Molesky, C. J. Dewalt, and Z. Jacob, "High temperature epsilon-near-zero and epsilon-near-pole metamaterial emitters for thermophotovoltaics," Opt. Express **21**(S1 Suppl 1), A96–A110 (2013).
18. I. Celanovic, N. Jovanovic, and J. Kassakian, "Two-dimensional tungsten photonic crystals as selective thermal emitters," Appl. Phys. Lett. **92**(19), 193101 (2008).
19. Y. X. Yeng, M. Ghebrebrhan, P. Bermel, W. R. Chan, J. D. Joannopoulos, M. Soljačić, and I. Celanovic, "Enabling high-temperature nanophotonics for energy applications," Proc. Natl. Acad. Sci. U.S.A. **109**(7), 2280–2285 (2012).
20. V. Stelmakh, V. Rinnerbauer, R. D. Geil, P. R. Aimone, J. J. Senkevich, J. D. Joannopoulos, M. Soljačić, and I. Celanovic, "High-temperature tantalum tungsten alloy photonic crystals: Stability, optical properties, and fabrication," Appl. Phys. Lett. **103**(12), 123903 (2013).
21. V. Rinnerbauer, S. Ndao, Y. X. Yeng, W. R. Chan, J. J. Senkevich, J. D. Joannopoulos, M. Soljačić, and I. Celanovic, "Recent developments in high-temperature photonic crystals for energy conversion," Energy Environ. Sci. **5**(10), 8815 (2012).
22. V. Rinnerbauer, S. Ndao, Y. X. Yeng, R. D. Geil, J. J. Senkevich, K. F. Jensen, J. D. Joannopoulos, M. Soljačić, and I. Celanovic, "Large-area fabrication of high aspect ratio tantalum photonic crystals for high-temperature selective emitters," J. Vac. Sci. Technol. B **31**(1), 011802 (2013).
23. V. Rinnerbauer, Y. X. Yeng, W. R. Chan, J. J. Senkevich, J. D. Joannopoulos, M. Soljačić, and I. Celanovic, "High-temperature stability and selective thermal emission of polycrystalline tantalum photonic crystals," Opt. Express **21**(9), 11482–11491 (2013).
24. C. Neff and C. Summers, "A photonic crystal superlattice based on triangular lattice," Opt. Express **13**(8), 3166–3173 (2005).
25. T. Utikal, T. Zentgraf, S. G. Tikhodeev, M. Lippitz, and H. Giessen, "Tailoring the photonic band splitting in metallodielectric photonic crystal superlattices," Phys. Rev. B **84**(7), 075101 (2011).
26. M.-L. V. Tse, Z. Liu, L.-H. Cho, C. Lu, P.-K. A. Wai, and H.-Y. Tam, "Superlattice microstructured optical fiber," Materials **7**(6), 4567–4573 (2014).
27. D. M. Callahan, K. A. Horowitz, and H. A. Atwater, "Light trapping in ultrathin silicon photonic crystal superlattices with randomly-textured dielectric incouplers," Opt. Express **21**(25), 30315–30326 (2013).
28. M. Ghebrebrhan, P. Bermel, Y. X. Yeng, I. Celanovic, M. Soljačić, and J. D. Joannopoulos, "Tailoring thermal emission via Q matching of photonic crystal resonances," Phys. Rev. A **83**(3), 033810 (2011).
29. V. Liu and S. Fan, "S⁴: A free electromagnetic solver for layered periodic structures," Comput. Phys. Commun. **183**(10), 2233–2244 (2012), http://www.stanford.edu/group/fan/S4/.
30. A. F. Oskooi, D. Roundy, M. Ibanescu, P. Bermel, J. D. Joannopoulos, and S. G. Johnson, "Meep: A flexible free-software package for electromagnetic simulations by the FDTD method," Comput. Phys. Commun. **181**(3), 687–702 (2010), http://ab-initio.mit.edu/meep.
31. Y. S. Touloukian and D. P. DeWitt, *Thermophysical Properties of Matter: Thermal Radiative Properties* (Plenum, 1970, Vol. 7).
32. P. Bermel, M. Ghebrebrhan, W. Chan, Y. X. Yeng, M. Araghchini, R. Hamam, C. H. Marton, K. F. Jensen, M. Soljačić, J. D. Joannopoulos, S. G. Johnson, and I. Celanovic, "Design and global optimization of high-efficiency thermophotovoltaic systems," Opt. Express **18**(S3 Suppl 3), A314–A334 (2010).
33. S. Y. Chou, P. R. Krauss, and P. J. Renstrom, "Imprint of sub-25 nm vias and trenches in polymers," Appl. Phys. Lett. **67**(21), 3114 (1995).
34. H. Schift, "Nanoimprint lithography: An old story in modern times? A review," J. Vac. Sci. Technol. B **26**(2), 458 (2008).
35. N.-P. Harder and P. Würfel, "Theoretical limits of thermophotovoltaic solar energy conversion," Semicond. Sci. Technol. **18**(5), S151–S157 (2003).
36. A. Datas and C. Algora, "Global optimization of solar thermophotovoltaic systems," Prog. Photovolt. Res. Appl. **21**, 1040–1055 (2013).
37. M. W. Dashiell, J. F. Beausang, H. Ehsani, G. Nichols, D. M. DePoy, L. R. Danielson, P. Talamo, K. D. Rahner, E. J. Brown, S. R. Burger, P. M. Fourspring, W. E. Topper, Jr., P. Baldasaro, C. A. Wang, R. K. Huang, M. K. Connors, G. W. Turner, Z. A. Shellenbarger, G. Taylor, J. Li, R. Martinelli, D. Donetski, S. Anikeev, G. L. Belenky, and S. Luryi, "Quaternary InGaAsSb thermophotovoltaic diodes," IEEE Trans. Electron. Dev. **53**(12), 2879–2891 (2006).

38. W. Chan, R. Huang, C. Wang, J. Kassakian, J. Joannopoulos, and I. Celanovic, "Modeling low-bandgap thermophotovoltaic diodes for high-efficiency portable power generators," Sol. Energy Mater. Sol. Cells **94**(3), 509–514 (2010).
39. Y. X. Yeng, W. R. Chan, V. Rinnerbauer, J. D. Joannopoulos, M. Soljačić, and I. Celanovic, "Performance analysis of experimentally viable photonic crystal enhanced thermophotovoltaic systems," Opt. Express **21**(S6 Suppl 6), A1035–A1051 (2013).

1. Introduction

A spectrally selective solar absorber is a critical element for solar thermal and solar thermophotovoltaic (STPV) applications [1–4]. To achieve high efficiencies in these energy conversion processes high operating temperatures well above 1000K are advantageous. In the high temperature regime, spectral selectivity is especially critical since the power lost by radiation from the absorber surface increases with the 4th power of the surface temperature. Therefore, it is imperative to have high solar absorptivity and at the same time to keep the losses due to re-emission by the absorber surface low [5,6]. Thermal stability of all components and of the spectral properties of the absorber is another critical issue at these high target operating temperatures [6]. Several approaches to highly selective absorbers based on impedance matching, metamaterials and photonic crystals have been proposed and demonstrated [4–13] but there is still room for improvement. For example, using 2D PhCs in refractory metals offers advantages of easy fabrication and high thermal stability [18–20]. Yet the spectral range of high absorptivity is limited, mostly due to diffraction losses of the periodic lattice in the short wavelength range. In this paper we show how the high absorptivity range of a solar absorber can be extended and tuned using a superlattice PhC design. The design consists of two superposed lattices with different cavity radii, i.e. a lattice with more than one cavity per unit cell. In this case, the contribution from modes of both cavities extends the spectral range of high absorptivity, which can be tailored by changing the geometrical parameters of the cavities. The geometry, i.e. the diameter of the cavities, is optimized first for the target operating parameters of a realistic STPV system with a moderate concentration of 250 suns and a target operating temperature of 1500K. The figure of merit is the thermal transfer efficiency of the absorber, which takes into account the solar absorptivity and the thermal emissivity of the absorber for the specific set of operating conditions. Next, high concentration solar applications are studied, where a broadband high absorptivity is desirable and has a higher impact on the thermal transfer efficiency than a low thermal emissivity. Excellent solar absorptivity can be achieved using a superlattice design with polygonal cavities and including an antireflection coating. This design is optimized for system parameters of 1000 suns and 1500K, achieving a solar absorptivity of 96.2% and a thermal transfer efficiency of 82.9%.

Finally, we study the performance of an STPV system with the superlattice PhC absorber. The emitter consists of a 2D PhC optimized for a photovoltaic (PV) cell with a bandgap at λ_{PV} = 2.3 μm (0.54 eV). In a detailed model, all the losses of the system in dependence of temperature are included and the irradiance needed to achieve the operating temperature is calculated from the power balance of the system and the solar absorptivity of the absorber. The largest contribution to system losses is by reflection and re-emission on the absorber side. To minimize re-emission, the absorber-to-emitter area ratio, e.g. the structured area of the absorber, can be reduced. In addition, a high reflectivity aperture from Ag can be used as an additional filter on the absorber side. The influence of both measures on the optical conversion efficiency and the system efficiency is studied and compared for a simple lattice absorber, the superlattice absorber and a blackbody-like absorber. The results show that the optical conversion efficiency of the absorber-emitter pair, i.e. the ratio of useful output radiation vs. incident irradiance, can be more than doubled by reducing the absorber-to-emitter area ratio and using the mirror aperture.

2. Solar absorber with 2D PhC superlattice

2.1 Design approach

A simple design to achieve high spectral selectivity is a 2D PhC consisting of a square array of cylindrical cavities etched into a tantalum (Ta) substrate [21]. This design has the advantage of a simple, scalable fabrication route using e.g. interference lithography, and the promise of high thermal stability using an additional surface coating of HfO_2 as shown in a previous study [22,23]. The enhanced spectral absorptance in this PhC absorber as compared to the flat substrate is achieved due to the efficient coupling of incident light into resonant electromagnetic modes supported by the PhC cavities. The absorption peak and the cutoff wavelength between the spectral range of high and low absorptance are approximately given by the fundamental mode of the metallic cavity and can therefore be tuned by the geometry of the cavity. The spectral bandwidth of this design and therefore the solar absorptivity is limited due to the number of supported cavity modes and by diffraction. The latter occurs at wavelengths smaller than the period of the lattice, which is usually in the visible range.

To maximize the bandwidth of the solar absorber and therefore the solar absorptivity, we propose a PhC superlattice design consisting of a unit cell with more than one cavity. PhC superlattices have been used to achieve superior control over bandgap, band dispersion and the density of optical states [24–27]. In this study, the enhanced spectral control is achieved through a wider spectrum of cavity modes. The introduction of another cavity with a second, smaller radius in the unit cell enforces an absorption peak at shorter wavelengths. By tuning the radii of the two cavities, we can set the absorption peak of the second cavity into the spectral range where the first cavity shows diffraction. Thus, the decrease of absorption from diffraction by the first cavity with larger radius is avoided and the spectral bandwidth of the absorber enlarged. In the long wavelength range, the spectral absorptance can be described by the surface-area weighted impedance, and thus depends mainly on the filling factor of the cavities [28]. In the long-wavelength limit, the free electron density makes the dominant contribution to the permittivity, and effective medium theory is valid. Decreasing the fraction of the metal decreases the free electron density. This lowers the effective plasma frequency, which increases the emissivity.

The numerical simulations of the spectral properties of the PhCs were performed using a rigorous coupled wave analysis (RCWA) algorithm implemented via S4 [29] and verified by a finite difference time domain algorithm (FDTD) implemented via MEEP [30]. Although both algorithms are not ideal for metals, good convergence was achieved with increasing number of Fourier expansion modes and resolution, respectively. The material properties of Ta as the substrate material are taken into account using the dispersion of Ta at high temperature taken from literature [31].

To demonstrate the concept of the superlattice PhC absorber, we study the case of a square lattice with cylindrical cavities with radius r_1 and period a and improve its absorptance by introducing a second cavity with radius r_2. The simulated absorptance spectra for normal incidence are shown in Fig. 1. The spectral response of the simple square lattice with one cavity with radius $r_1 = 0.28$ μm, a period $a = 0.66$ μm and a cavity depth of $d = 4.6$ μm is compared to that of a simple square lattice with one cavity with radius $r_2 = 0.12$ μm and a smaller period of $a_2 = a/\sqrt{2} = 0.47$ μm. In both cases, the spectral absorptance shows a maximum at a wavelength corresponding to approximately twice the diameter of the cavity. For wavelengths smaller than the period of the lattice, the reflectance increases due to the contribution of diffraction and the absorptance drops – in the case of the first PhC lattice exactly in the range of the maximum of the solar spectrum around 500 nm. The spectral response of a superlattice PhC combining both lattices, i.e., consisting of a square lattice of period a with two cavities with radii r_1 and r_2 in the unit cell, however shows the absorptance maxima of both cavities and therefore a wider absorption bandwidth and higher solar

absorptivity. The solar absorptivity $\bar{\alpha}$ is defined as the weighted average over the incident solar spectrum:

$$\bar{\alpha} = \frac{1}{H_S} \int_0^\infty d\lambda \, \varepsilon(\lambda) S_S(\lambda), \tag{1}$$

where $S_s(\lambda)$ is the solar spectrum (AM1.5D), H_S is the total solar irradiance, $\varepsilon(\lambda)$ is the spectral emittance of the absorber and λ is the wavelength of light. With the superlattice design the solar absorptance is increased from 0.80 for the simple lattice to 0.85 (both at normal incidence).
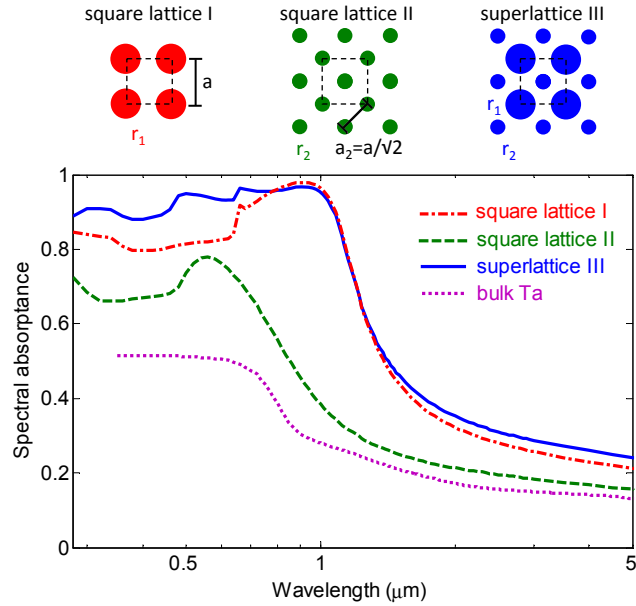

Fig. 1. Normal spectral absorptance for square lattice and superlattice with period $a = 0.66$ μm, radius $r_1 = 0.28$ μm and $r_2 = 0.12$ μm and depth $d = 4.6$ μm, and absorptance for bulk Ta at 1478 K [31] for comparison. Schematics of the lattices are shown for all PhC designs.

Due to the angular dependence of the spectral absorptance of the PhC the solar absorptivity decreases with increasing opening angle of the incident light. The decrease in solar absorptivity, however, is below 1% up to an opening (half) angle of 30° both for the simple lattice as well as for the superlattice. With an acceptance angle of 30° on the absorber side, a concentrator can exceed a concentration of 10000 suns, following the conservation of etendue and using the solid angle of the unconcentrated direct sunlight, which is 68.5 μSr or 0.267°. In case the incident angle on the concentrating system is not normal, a larger acceptance angle might be beneficial. But if the acceptance angle of the absorber is increased from 30° to full hemispherical irradiation, the improvement of the acceptance angle of the concentrator is only a factor of two. Therefore the angular dependence of the solar absorptivity can be neglected in this design and we restrict the following discussion to the case of normal incidence on the absorber.

2.2 Thermal transfer efficiency

For high temperature applications, it is critical to minimize the losses due to re-emission by the solar absorber, as discussed before. Therefore, there is a trade-off between the solar absorptivity $\bar{\alpha}$ and the thermal emissivity $\bar{\varepsilon}(T)$ of the absorber, which is defined as

$$\bar{\varepsilon} = \frac{\int_0^\infty d\lambda \, \varepsilon(\lambda) / \{\lambda^5 (e^{\frac{hc}{\lambda kT}} - 1)\}}{\int_0^\infty d\lambda / \{\lambda^5 (e^{\frac{hc}{\lambda kT}} - 1)\}}, \tag{2}$$

where T is the operating temperature, h is the Planck constant, c is the speed of light and k is the Boltzmann constant. To calculate this thermal emissivity, the hemispherical spectral emittance $\varepsilon(\lambda)$ of the PhC is used. For the superlattice design there is a small increase in the spectral emittance at long wavelengths as compared to the simple lattice PhC (see Fig. 1). As discussed before, this is due to the increased fill factor of the cavities, which leads to higher thermal emissivity. As shown in Fig. 2(a) both the solar absorptivity and the thermal emissivity at 1500 K increase with increasing cavity radius r_2.

The figure of merit for the optimization of the solar absorber is therefore the thermal transfer efficiency η_T which is defined as the difference between input and output power normalized to the incident power [32]:

$$\eta_T = \bar{\alpha} - \bar{\varepsilon} \cdot \frac{\sigma T^4}{H_s}, \tag{3}$$

with the solar absorptivity $\bar{\alpha}$ and the thermal emissivity $\bar{\varepsilon}$ as defined above, H_S is the total solar irradiance, and σ being the Stefan-Boltzmann constant. The maximum of the thermal transfer efficiency therefore depends on the operating conditions of incident solar irradiance (concentration) and operating temperature. The geometry of the superlattice PhC absorber is first optimized for realistic operating parameters of an STPV system with an operating temperature of 1500 K and a moderate incident irradiance of 250 kW/m^2 (i.e., 250 suns, AM1.5 direct). In Fig. 2(b) the thermal transfer efficiency of the superlattice absorber is shown as a function of the cavity radii r_1 and r_2. The maximum $\eta_T = 0.472$ is achieved for $r_1 = 0.28$ μm, $r_2 = 0.12$ μm and period $a = 0.66$ μm. In comparison, the simple square lattice optimized for the same system conditions has $r_1 = 0.28$ μm and period $a = 0.66$ μm and achieves only $\eta_T = 0.452$. The solar absorptivity $\bar{\alpha}$ is increased from $\bar{\alpha} = 80.2\%$ to $\bar{\alpha} = 85.0\%$ using the superlattice PhC absorber. Note that the cavity depth only has a secondary effect on the spectral properties and the efficiency and is therefore kept constant at $d = 4.6$ μm. Also, the fabrication limitations are taken into account by ensuring a minimum distance of 25 nm between the cavities.
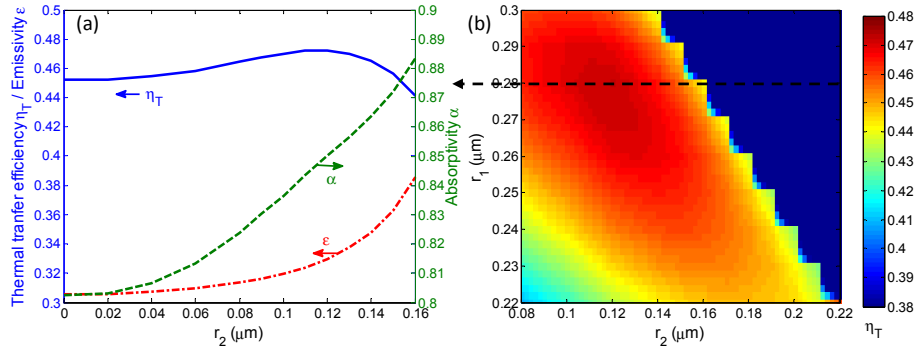

Fig. 2. (a) Thermal transfer efficiency η_T and thermal emissivity ε at 1500 K and solar absorptivity α for PhC absorbers with $r_1 = 0.28$ μm and increasing radius r_2 of the superlattice cavities. (b) Thermal transfer efficiency at 1500 K and 250 suns for the superlattice absorber with period $a = 0.66$ μm and depth $d = 4.6$ μm in dependence of the cavity radii.

2.3 Broadband solar absorber

The superlattice PhC offers large freedom of design to tailor the spectral absorptance with the geometry of the cavities and to optimize the structure according to the system requirements. As discussed above, the relative influence of the solar absorptivity and the thermal emissivity on the thermal transfer efficiency depends on the operating conditions of incident irradiance and temperature. For the case of high concentration systems, the impact of the solar absorptivity is critical and broadband high absorptivity is desirable. In this case, designs with large cavities are favored since they increase the absorptivity over a broad spectral range. Using polygonal cavities we can increase the diameter of the cavities and their fill factor as compared to the cylindrical cavity superlattice, maximizing the number of available cavity modes in the unit cell and achieving higher efficiencies for high concentration systems. In Fig. 3 we show the normal spectral absorptance of the superlattice with cavities consisting of polygons, as shown in the schematic in the inset. In this design the unit cell consists of an octagon and a square, where r_1 and r_2 denote their respective circumferences. We include a surface coating of 40 nm HfO_2 as an antireflective coating, which is optimized to enhance the spectral absorptance in the visible range. Including this coating already improves the solar absorptivity for the simple lattice PhC [6] while also ensuring high temperature stability [23]. Using the superlattice design with the coating we can substantially extend the bandwidth of high spectral absorptance into the infrared, as shown in Fig. 3. Design 4 was optimized for maximum thermal transfer efficiency at 1000 suns and 1500 K. The optimized period is $a = 1$ µm and radii $r_1 = 0.49$ µm and $r_2 = 0.24$ µm with a cavity depth of $d = 4.6$ µm, including a conformal coating of 40 nm HfO_2. With this design, the solar absorptivity is increased by 10% to $\bar{\alpha} = 96.2\%$ from $\bar{\alpha} = 86.4\%$ for the simple square lattice PhC absorber (design 1, cylindrical cavities) with $a = 0.66$ µm and radius $r_1 = 0.24$ µm with the same antireflective coating. The thermal transfer efficiency is increased to $\eta_T = 0.829$ for the superlattice absorber as compared to $\eta_T = 0.780$ for the simple square lattice PhC absorber. (Note that for moderate concentrations, the performance of the cylindrical and the polygonal PhC is comparable). Large-scale fabrication of such a polygonal superlattice PhC is feasible using e.g. nanoimprint lithography [33,34].
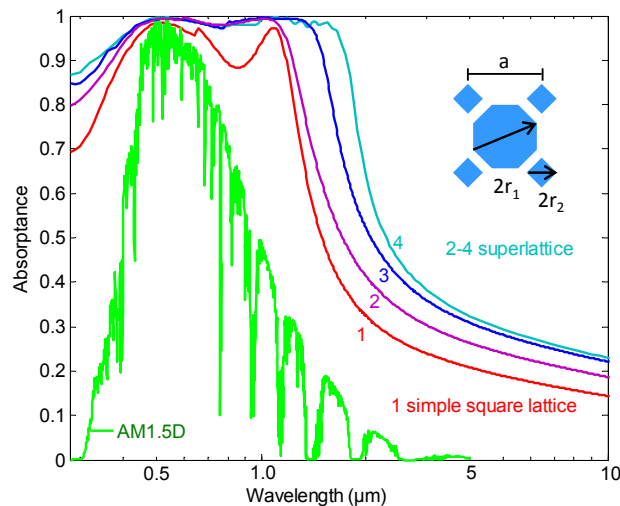
Fig. 3. Normal spectral absorptance for: 1 the square lattice (cylindrical) PhC with $a = 0.66$ µm, $r_1 = 0.24$ µm, and (polygonal) superlattice with 2: $a = 0.6$ µm, $r_1 = 0.27$ µm, $r_2 = 0.1$ µm, 3: $a = 0.8$ µm, $r_1 = 0.39$ µm, $r_2 = 0.15$ µm, 4: $a = 1.0$ µm, $r_1 = 0.49$ µm, $r_2 = 0.24$ µm; all with cavity depth $d = 4.6$ µm and antireflection coating of 40 nm HfO_2, and solar spectrum AM1.5D (green trace).

3. Optimized STPV system

In the next step, the performance of the superlattice absorber is studied in a high concentration STPV system, and the influence of several system parameters on the system performance is determined. In the STPV system, a conversion step consisting of a combined solar absorber and thermal emitter converts the incident solar radiation into thermal radiation that is ideally matched to the bandgap of a small bandgap PV cell. The system performance depends on a detailed balance of the incident irradiance and the output power through all loss channels, which determines the operating temperature reached. For a more detailed discussion see [35,36]. At high temperatures, losses taking place on the absorber side have a critical impact on the system performance. In an earlier study it was shown for an experimental STPV setup that approximately 50% of the incident power density, depending on operating parameters, are already lost on the absorber side either by reflection (insufficient absorption) or re-emission (high thermal losses) [6]. Figure 4(a) shows a schematic sketch of an STPV system design with a planar absorber/emitter pair, where the system is specifically optimized to minimize losses on the absorber side. The broadband superlattice absorber with antireflective coating significantly helps to reduce losses due to reflection. By reducing the absorber area with respect to the emitter area, losses by re-emission of the absorber can be reduced [1,35]. In the planar absorber/emitter design the structured absorber-to-emitter area ratio *AR* is optimized, while the remaining area of the absorber side is unstructured and its emissivity is that of the flat polished substrate. In addition, a high reflectance aperture (e.g. Ag) with an aperture size equal to the structured absorber area is used to recycle thermal emission from the absorber.

3.1 System model

A detailed model including all the losses is implemented to predict system performance and to optimize the system parameters as well as the absorber design. In this model the emitter is a 2D Ta PhC as described in an earlier study [6] and matched to an InGaAsSb cell, which has a bandgap at λ_{PV} = 2.3 μm (0.54 eV) [37]. Further, the model is based on isothermal operation of the absorber/emitter pair, i.e., absorber and emitter being at the same operation temperature. To calculate the incident irradiance on the absorber that is needed to reach a target operating temperature, we take into account the solar absorptivity of the absorber, the radiative losses from all surfaces (absorber, emitter, sides and support needles) and conduction losses through the supporting needles holding the absorber/emitter pair. Thermal re-emission on the absorber side is calculated for the case without and with Ag aperture, taking into account multiple reflections and the geometry of the sample, assuming a gap of 300 μm to the aperture. We study system performance for an experimental setup where the area of the absorber/emitter pair and the matched PV cell is 1 cm^2 as well as for a more efficient large scale case with an area of 100 cm^2.

The photon flux from the emitter incident on the PV cell is calculated from the hemispherical spectral emittance of the emitter for different temperatures. The geometry, i.e., the finite size of the emitter and PV cell and the gap between them, resulting in cavity losses, is included via the viewfactor assuming a gap of 300 μm. In addition, the radiation reflected back from the PV cell to the emitter is included in the model. In the useful wavelength range (i.e. below the cutoff wavelength of the PV cell) the measured reflectance of the PV cell is taken into account. Above the cutoff wavelength, the influence of the PV cell reflectance is studied by assuming different reflectance values R_{PV}.

As a measure of the performance of the optical conversion stage we define the optical efficiency η_{opt} as the ratio of useful irradiance from the emitter reaching the PV cell (i.e. below the cutoff wavelength of the PV cell) to the overall incident irradiance:

$$\eta_{opt} = \frac{F_V}{H_S} \int_{\lambda_{min}}^{\lambda_{PV}} d\lambda \, \varepsilon_{eff}(\lambda) \frac{2\pi h c^2}{\lambda^5 (e^{\frac{hc}{\lambda kT}} - 1)}, \tag{4}$$

$$\eta_{STPV} = \eta_{opt} \cdot \eta_{PV}, \tag{5}$$

where ε_{eff} is the effective spectral emittance of the emitter, taking into account back-reflection from the PV cell, F_V is the viewfactor, λ_{min} and λ_{PV} are the lower and upper limits of the quantum efficiency of the PV cell, denoting the useful wavelength range. As the irradiance reaching the PV cell only depends on the emitter T (for a given emitter), the optical efficiency therefore depends directly on the irradiance needed to reach this operating T. The overall system efficiency η_{STPV} is the product of optical efficiency η_{opt} and the electrical efficiency of the PV cell η_{PV}. In our model we determine the system efficiency as the ratio of electrical output power to the incident solar power, where the electrical output power is calculated for a real InGaAsSb cell using the PV parameters determined from the measured I-V curve [38].
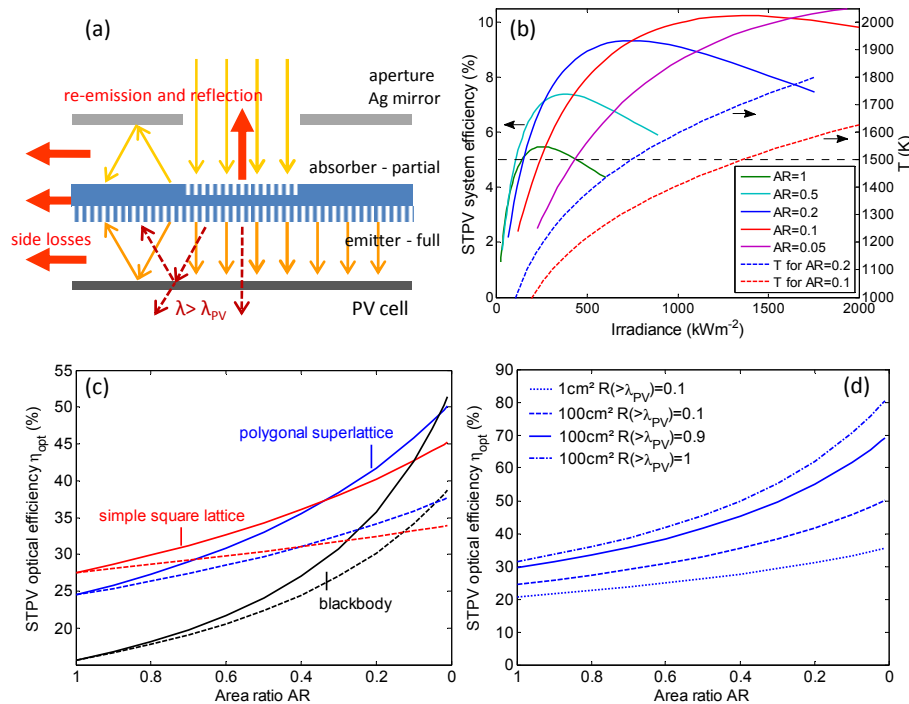

Fig. 4. (a) Schematic of the STPV configuration with area-optimized absorber/emitter pair and aperture. (b) STPV system efficiency dependence on incident irradiance for different AR using the polygonal superlattice PhC absorber (design 4) with Ag aperture and PhC emitter matched to an InGaAsSb PV cell ($\lambda_{PV} = 2.3\mu m$), and measured cell efficiency η_{PV}. System temperature T for the same system in dependence of irradiance (dashed lines, right axis). (c) Optical conversion efficiency η_{opt} of superlattice PhC, square lattice PhC and blackbody absorber with Ag aperture (solid lines) and without (dashed) for different AR at 1500K. (d) η_{opt} of superlattice PhC absorber for different STPV system configurations, all at 1500K with Ag aperture vs. absorber-to-emitter area ratio AR. The different cases were calculated for small scale 1 cm^2 and large scale 100 cm^2 device areas, and different reflection coefficients R_{PV} on the PV cell side.

3.2 Optimizing the absorber area

In Fig. 4(a) the STPV system model is shown including the main radiation channels. In the following, the influence of the main loss mechanisms and the improvements by optimizing

the absorber area are discussed. One loss mechanism that can be addressed and minimized on a system level are the side losses by radiation from the sides of the absorber-emitter pair and by radiation escaping through the gaps between the absorber-emitter pair and the Ag aperture on the front, and the PV cell on the back, respectively. These side losses can be substantially reduced by upscaling of the setup, i.e. increasing the area of the absorber-emitter pair and of the matching PV cell. In the system model, losses by radiation and conduction of the support holding the absorber-emitter pair are also taken into account. Modeling shows that for a large-scale device with a minimum amount of small support needles, these losses can be kept well below 1%. A crucial loss channel is the parasitic emission of the emitter above the bandgap wavelength λ_{PV} of the PV cell, which cannot be converted to electricity and is lost as waste heat. By design, the 2D Ta PhC emitter optimized for a PV cell with $\lambda_{PV} = 2.3$ µm used in this model has a spectral selectivity of $\eta_{sp} = 57\%$ at 1500 K, i.e., 57% of the emitted radiation is below the cutoff wavelength λ_{PV}. By using a cold-side filter or engineering the reflection of the PV cell, the radiation above the cutoff wavelength can be reflected back to the emitter and reabsorbed, increasing the spectral efficiency of the emitter and the system efficiency. Losses on the absorber side due to reflection and re-emission can be substantially reduced by optimizing the absorber-to-emitter area AR and using a high-reflectivity aperture on the front side.

As shown in Fig. 4(b) there is an optimum area ratio AR for a given irradiance, since the irradiance needed to reach a target operating temperature increases for smaller absorber areas. The calculated system efficiency η_{STPV} is compared for a 100 cm^2 absorber/emitter pair with a polygonal superlattice absorber (Design 4 in Fig. 3), an Ag aperture and different area ratios AR in dependence of the incident irradiance. Note that the optimum operating temperature (and therefore, irradiance) is determined mostly by the performance of the PV cell. In this calculation the measured performance of an InGaAsSb cell is used [38]. The efficiency η_{PV} of this PV cell has a maximum of 24.8% at approximately 1300K and then decreases with increasing operating temperature, i.e., increasing irradiance from the emitter, due to losses connected to the series resistance [6]. For this PV cell and the PhC emitter used in the model, the system efficiency reaches its maximum at T = 1500K (Fig. 4(b)). At 1500K the efficiency of the measured PV cell is $\eta_{PV} = 22.6\%$ compared to 51.1% for an ideal PV cell [39]. As can be seen, the incident irradiation (concentration) needed to reach this optimum T, and therefore maximum system efficiency, increases with decreasing area ratio AR. In the calculated system efficiency shown in Fig. 4(b) the reflection from the PV cell above the cutoff wavelength was assumed to be $R_{PV} = 0.1$ (not optimized). Still, we can achieve an STPV system efficiency above $\eta_{STPV} > 10\%$ for an irradiance above 1000 suns using a coated superlattice absorber with $AR \leq 0.1$. Using a cold side filter that reduces reflection on the PV cell with $R_{PV} = 0.9$ for wavelengths above the cut-off $\lambda_{PV} = 2.3$ µm the system efficiency η_{STPV} can exceed 20% for $AR \leq 0.1$.

In Fig. 4(c) we further study the influence of the reduced area ratio and of the Ag aperture on the optical efficiency η_{opt} as defined in Eq. (4) for the case of the simple square absorber with cylindrical cavities, the polygonal superlattice absorber (design 4) and a blackbody-like absorber (with $\alpha = \varepsilon = 1$), all with a sample area of 100 cm^2 and $R_{PV} = 0.1$ at an operating temperature of 1500K. At a high area ratio, i.e., low incident concentration, the calculated optical efficiency is highest for the square lattice absorber since it has lower thermal emissivity. For $AR = 1$ (the absorber covers the front surface area completely) the optical efficiency is $\eta_{opt} = 27.5\%$ with the simple square lattice absorber, which requires an incident irradiance of 226 suns to reach the optimum system T = 1500K, as compared to 24.5% for the superlattice absorber (254 suns) and 15.6% for the blackbody absorber (398 suns), respectively. For decreasing area ratio the optical efficiency increases: the remaining unstructured area has a lower thermal emittance and therefore losses due to re-emission are smaller, even without Ag aperture (dashed lines in Fig. 4(c)). With decreasing AR the superlattice absorber gains over the square lattice absorber since firstly, the thermal

emissivity is decreased, and secondly, the concentration is increased and the impact of the higher solar absorptivity on the optical efficiency is more relevant. Without Ag aperture, the optimized superlattice absorber has a higher optical efficiency than the square lattice for approximately $AR<0.4$. At $AR = 0.1$ the superlattice absorber achieves η_{opt} = 35.9%, requiring an incident irradiance of 1731 suns to reach a system T = 1500K, as compared to the blackbody absorber with η_{opt} = 34.1% (1820 suns) and the square lattice absorber with 33.2% (1872 suns). Including the Ag aperture in the system design (solid lines in Fig. 4(c)) the re-emission from the remaining area is reflected back and is re-absorbed, which reduces thermal losses from the absorber side even further for $AR< 1$. In fact, in this case the losses by re-emission are mostly governed by the reflectance of the aperture (and the viewfactor on the absorber side) i.e., even if the whole area below the Ag mirror is structured we can achieve almost the same optical efficiency as for the case where the structured absorber is limited to the illuminated area. With the Ag aperture, the superlattice absorber achieves η_{opt} = 45.8% at $AR = 0.1$, and reducing the required irradiance of 1357 suns to reach 1500K, as opposed to the square lattice absorber with η_{opt} = 42.7% (1455 suns) and the blackbody absorber with η_{opt} = 42.6% (1460 suns). Although the solar absorptivity of the superlattice absorber of $\bar{\alpha}$ = 96.2% is slightly smaller than that of a blackbody, the superlattice absorber still achieves higher optical efficiencies than a blackbody-like absorber for AR above about 0.02.

In Fig. 4(d) the calculated optical conversion efficiency is shown for different system parameters versus the absorber-to-emitter area ratio. In this comparison, the superlattice PhC absorber design 4 is used including an Ag aperture and at an operating temperature of 1500K. Different cases are compared where losses are reduced step by step: first, a small scale device of 1 cm^2, and low reflectance of the PV cell side R_{PV} = 0.1 for wavelengths above λ_{PV} = 2.3 μm. Second, scaling up to an area of 100 cm^2 in which case the side losses are substantially reduced. By increasing the reflectance R_{PV} in the long wavelength range to R_{PV} = 0.9 in case 3 and R_{PV} = 1 in case 4 the losses by parasitic emission of the emitter are substantially reduced and the spectral selectivity of the emitter is improved. In this case, the optical efficiency η_{opt} is dominated by losses due to re-emission and reflection by the absorber. By reducing the area ratio of absorber-to-emitter AR, the optical efficiency η_{opt} is dramatically increased. More than η_{opt} = 80% are achieved for an ideal cold side filter with R_{PV} = 1 and a small $AR \leq 0.02$ with an Ag front side aperture (at a concentration of ≥5300 suns). The system efficiency for this case, using an ideal PV cell with a bandgap wavelength of λ_{PV} = 2.3 μm and an efficiency η_{PV} = 51.1% at 1500K can exceed η_{STPV} = 40% for operating temperatures ≥1500K. Using a cold side filter with R_{PV} = 0.9, the optical efficiency is almost 70% and the system efficiency can exceed η_{STPV} = 20% for T≥1500K even with the PV cell used in the experiment. For the measured PV cell and R_{PV} = 0.1, the optical efficiency can still be doubled by reducing AR and using the mirror aperture, and reach η_{opt} = 50% for the large-scale case of 100 cm^2, albeit at the cost of increased irradiance required to reach the optimum operating temperature of 1500K from 254 suns at $AR = 1$ to 6263 suns at $AR = 0.02$.

4. Conclusion

A superlattice PhC design is studied to achieve broadband high spectral absorptance in the solar spectrum range, while retaining low emittance in the long wavelength range. This high selectivity is crucial for applications at the high operating temperatures (> 1000K) which are necessary to achieve high efficiencies in energy conversion applications. When using a simple square lattice PhC, the range of high absorptivity, i.e., low reflectivity, is limited due to diffraction which occurs at wavelengths below the period of the lattice. The superlattice PhC absorber achieves broadband solar absorption due to the contribution from two cavities with different radii per unit cell. The spectral range of high absorptivity can be tuned by the geometry of the cavities. At the same time, the design can retain low emittance, i.e., high reflectivity, in the long wavelength range, which is important at high operating temperatures to keep thermal emissivity and therefore losses due to re-emission low.

The superlattice PhC design is optimized for a low concentration system of 250 suns and an operating temperature of 1500K. Using a superlattice consisting of two cylindrical cavities per unit cell, the solar absorptivity is improved by 5% from 80% to 85% compared to the simple lattice. The thermal transfer efficiency, as a measure of the performance of the absorber is improved by 2% from 45.2% to 47.2% for this case. For the case of a high concentration system, the solar absorptivity has a higher impact on the thermal transfer efficiency of the absorber. In this case, a superlattice PhC consisting of polygonal cavities is used together with an additional antireflection coating of 40 nm HfO_2. The design is optimized for an irradiance of 1000 suns and an operating temperature of 1500K. The thermal transfer efficiency for the optimized design is 82.9% which is 5% higher than for the simple lattice PhC absorber with the same antireflection coating. The superlattice PhC achieves a high solar absorptivity of 96.2% which is an improvement of 10%.

Furthermore, the system performance of an STPV system using the superlattice absorber is studied. Using a highly reflecting Ag aperture as an additional entrance filter and optimizing the area ratio of absorber to emitter, the losses due to re-emission of the absorber can be minimized. The optical conversion efficiency of the STPV absorber-emitter stage with the spectral properties of the superlattice absorber and a PhC emitter optimized for a PV wavelength of 2.3 µm can reach up to 80%.

Acknowledgments